EPJ Web of Conferences **245**, 06036 (2020) https://doi.org/10.1051/epjconf/202024506036
CHEP 2019

On the direct detection of multi component dark matter

Andre Scaffidi[1,*]

[1]The University of Adelaide

Abstract. We study the case of multi-component dark matter, in particular how direct detection signals are modified in the presence of several stable weakly-interacting-massive particles. Assuming a positive signal in a future direct detection experiment, stemming from two dark matter components, we study the region in parameter space where it is possible to distinguish a one from a two-component dark matter spectrum. We leave as free parameters the two dark matter masses and show that the two hypotheses can be significantly discriminated for a range of dark matter masses with their splitting being the critical factor. For full details see the first of a series of two publications [1].

1 Introduction

We know from gravitational effects that dark matter (DM) constitutes a significant fraction of the energy density in the universe, but no confirmed detection in the laboratory has been made so far. Some of the most popular candidates are Weakly-Interacting-Massive-Particles (WIMPs), in particular those that have non-vanishing interactions with the standard model (SM) and therefore can be tested. In fact, they are actively being searched for in direct detection (DD) experiments, which look for their nuclear scatterings in underground detectors [2]. Interestingly, current and planned next-generation experiments are probing a very large portion of the parameter space of well-motivated theories of WIMPs.

A plausible scenario is that DM is not made up of a single species, but that it has a multi-component nature. In this work we study direct detection signals in the presence of multi-component WIMP-like DM, i.e., several types of WIMPs (labelled by Greek sub indices $\alpha = 1, 2 ..., N$) with individual global energy density Ω_α such that they constitute the observed total DM energy density of the Universe, $\Omega_{\rm DM} = \sum_\alpha^N \Omega_\alpha$. Purely on theoretical grounds, having the individual energy densities (the global Ω_α, or the local ρ_α) exactly equal would seem to be a highly unnatural scenario, requiring a fine-tuning between masses and number densities (unless there is some underlying mechanism to equalise the densities). On the other hand, that the densities are similar up to order one factors seems rather plausible, that is to say, that there are several species contributing in a non-negligible way to the global and local energy densities. For instance, in the SM there are baryons forming different stable nuclei with a non-negligible density: H, He, Li..., and also electrons, photons and neutrinos. Therefore, it is not difficult to imagine that a similar situation could occur in the dark sector, which has an energy density five times larger than the visible one.

There have been only a few works in the past regarding the direct detection of multi-component DM [3–9]. Let us discuss the main points studied there and the most relevant

*e-mail: Mailaddressforfirstauthor

differences with our analysis. In Ref. [4] the authors considered very small mass splittings (< 200 keV) for the particles, such as arise in inelastic scenarios [10–12]. In Ref. [5] a continuum spectrum of closely spaced DM particles was considered. In this work we will focus mainly on the case of two DM states and consider splittings comparable to the DM masses. In Refs. [5, 6] the possibility of testing multi-component DM using collider, indirect and direct searches was studied. In Ref. [6] the authors related the WIMP-nucleon scattering cross-section to the annihilation one, motivated by thermal freeze-out and supersymmetric scenarios. Therefore they were able to express the scattering cross-section as a function of the global (and local) density and the DM mass. In our study we will keep the analysis as phenomenological and model-independent as possible. In particular, we will not make any assumptions in the numerical analysis regarding the production mechanisms for the DM, i.e., we will keep the abundance and the scattering cross-sections as independent parameters. Furthermore, we will adopt a different statistical approach to that in Ref. [6] and we will study the effects of all relevant parameters entering the scattering rate. As pointed out in this last reference, indirect detection of one DM particle could mimic the effects of two components, as it may annihilate/decay not only to two gamma rays but also to Higgs/Z plus a photon. In addition these interactions are loop-suppressed. Regarding colliders, the authors studied the case of models with charged partners decaying into DM. In Ref. [13] the authors also considered the possibility of discriminating the number of DM particles generating missing energy distributions. In this work we will focus on how multi-component DM can be studied using only information stemming from direct detection signals.

2 Direct detection of multi-component DM

2.1 The differential event rate

We present in the following the general notation for multi-component DM in detectors with different types of nuclei. For the time-being, we assume elastic spin-independent (SI) scattering of DM particles χ_α ($\alpha = 1, 2 ..., N$) with masses m_α off nuclei with atomic and mass numbers (Z_j, A_j) ($j = 1, 2 ..M$), depositing the nuclear recoil energy E_R. The total differential rate (usually measured in events/keV/kg/day) observed by a detector is given by the sum of the event rates of the individual DM particles on each of the nuclear elements:

$$R(E_R, t) = \sum_{j=1}^{M} \sum_{\alpha=1}^{N} R_j^\alpha(E_R, t)\,, \tag{1}$$

where

$$R_j^\alpha(E_R, t) = x_j \frac{\rho_\alpha \sigma_\alpha^p}{2 m_\alpha \mu_{\alpha p}^2} (A_{\alpha,j}^{\rm eff})^2 F_j^2(E_R)\, \eta_{\alpha,j}(v_{m,j}^{(\alpha)}, t)\,, \tag{2}$$

with ρ_α the individual local DM energy density (with the restriction $\rho_{\rm loc} = \sum_{\alpha=1}^{N} \rho_\alpha$), σ_α^p the individual DM–proton scattering cross-section at zero momentum transfer, $\mu_{\alpha p}$ the χ_α particle–proton reduced mass and $F_j(E_R)$ the nuclear form factor of element j. We also denoted the effective mass-number of the nucleus j with DM α by

$$A_{\alpha,j}^{\rm eff} = Z_j + (A_j - Z_j)\kappa_\alpha\,, \tag{3}$$

with

$$\kappa_\alpha \equiv f_\alpha^n / f_\alpha^p\,, \tag{4}$$

where $f_\alpha^{n,p}$ are the SI individual couplings of the DM particle α to neutrons and protons. x_j is the mass fraction of element j in the detector, i.e., $x_j = m_j/(\sum_j^M m_j)$.

We will discuss spin-independent (SI) and spin-dependent (SD) interactions in this paper; in the case of SD interactions, Eq. (2) can be used by substituting $A_{\alpha j}^{\rm eff} \to 1$ and the form factor $F_j^2(E_R) \to F_{\alpha,j}^{\rm SD}(E_R, \kappa_\alpha)$ now has a κ_α dependence. In the numerical analysis, for the SI form factors we will use the Helm parametrisation [14, 15], while for SD in xenon (and fluorine) we will use the results of Ref. [16].

In addition to ρ_α, the astrophysics enters in Eq. (2) through the halo integral

$$\eta_{\alpha,j}(v_{m,j}^{(\alpha)}, t) \equiv \eta(f_{\rm det}^{(\alpha)}, v_{m,j}^{(\alpha)}, t) = \int_{v>v_{m,j}^{(\alpha)}} d^3v \frac{f_{\rm det}^{(\alpha)}(\mathbf{v}, t)}{v}\,, \tag{5}$$

with

$$v_{m,j}^{(\alpha)} \equiv v_m(m_\alpha,\, m_j) = \sqrt{\frac{m_j E_R}{2\mu_{\alpha j}^2}}, \tag{6}$$

where $v_{m,j}^{(\alpha)}$ is the minimal velocity of the particle α required to produce a recoil of energy E_R in element j, and $f_{\rm det}^{(\alpha)}(\mathbf{v}, t)$ describes the distribution of DM particle velocities in the detector rest frame, with $f_{\rm det}^{(\alpha)}(\mathbf{v}, t) \geq 0$ and $\int d^3v f_{\rm det}^{(\alpha)}(\mathbf{v}, t) = 1$. The velocity distributions in the rest frames of the detector and the galaxy are related by a Galilean transformation, $f_{\rm det}^{(\alpha)}(\mathbf{v}, t) = f_{\rm gal}^{(\alpha)}(\mathbf{v} + \mathbf{v}_e(t))$, where $\mathbf{v}_e(t)$ is the velocity vector of the Earth in the galaxy rest-frame. Notice that $\eta_{\alpha j}(v_{m,j}^{(\alpha)})$ is a decreasing function of $v_{m,j}^{(\alpha)}$, which for large DM masses does not depend on m_α. Throughout this paper, we will use the so-called Standard Halo Model (SHM), with $\rho_{\rm loc}^{\rm exp} \simeq 0.4\,{\rm GeV/cm^3}$, a Maxwellian velocity distribution $f_{\rm gal}(v) = \frac{1}{(2\pi\sigma_{H_\alpha}^2)^{3/2}} \exp\Big(-\frac{3v^2}{2\sigma_{H_\alpha}^2}\Big)$, and a cut-off at the escape velocity $v_{\rm esc} = 550\,{\rm km\,s^{-1}}$.

In principle, $\eta_{\alpha j}(v_{m,j}^{(\alpha)}, t)$ depends on the DM particle α in two different ways: directly, via its velocity distribution $f^{(\alpha)}(\mathbf{v}, t)$ (which, in addition may depend in a non-trivial way on the micro-physics of the DM, like its mass and interactions) and indirectly, through its mass m_α that enters into $v_{m,j}^{(\alpha)}$ (unless $m_\alpha \gg m_j$, in which case the dependence on the DM mass drops, $v_{m,j}^{(\alpha)} \to v_{m,j}$). In the following, we will assume that the functional form of the velocity distributions of the different DM components is equal, i.e., $f^{(\alpha)}(\mathbf{v}, t) \equiv f(\mathbf{v}, t)$. We will however consider the case of different velocity dispersions later on. Also, we will focus on constant rates, i.e., averaged over the year, so that

$$\bar{R}(E_R) = \frac{R(E_R, t_{\rm max}) + R(E_R, t_{\rm min})}{2}\,, \tag{7}$$

where $t_{\rm max}$ ($t_{\rm min}$) are the times of the year at which the rate reaches a maximum (minimum). [1]

2.2 The rate for two DM particles

We now fix the notation for the DD signals expected from 2 DM particles $\alpha = 1, 2$ with masses $m_1 < m_2$, cross-sections with protons σ_1^p, σ_2^p, and densities ρ_1, ρ_2, such that $\rho_1 + \rho_2 = \rho_{\rm loc}$. We will also study their signals in two different detectors $j = A_1, A_2$, with mass and atomic numbers $(A_1, Z_1) \neq (A_2, Z_2)$, and taken to have mass fractions $x_1 = x_2 = 1$ for

[1] We will not discuss annual modulation signals, the reader is referred to refs. [17–24] for studies on the topic.

simplicity (in the case of xenon, we will consider the different mass fractions of its isotopes). We define

$$r_\rho \equiv \frac{\rho_2}{\rho_1}\,, \qquad \text{such that} \qquad \rho_2 = r_\rho\,\rho_1 = r_\rho\,\frac{\rho_{\rm loc}}{1+r_\rho}\,. \tag{8}$$

From eqs. (1), (2) and (7) (dropping the bar from the notation of $R(E_R)$), and using $\mu_{1p} = \mu_{2p} = m_p$, we can write the total rate as:

$$\begin{aligned} R_1(E_R) &= R_1^1(E_R) + R_1^2(E_R) \\ &= C(r_\rho, \sigma_1^p)\, F_{A_1}^2(E_R)\left(\frac{(A_{1,1}^{\rm eff})^2}{m_1}\,\eta(v_{m,A1}^{(1)}) + \frac{(A_{2,1}^{\rm eff})^2}{m_2}\,r_\rho\, r_\sigma\,\eta(v_{m,A1}^{(2)})\right), \end{aligned} \tag{9}$$

where we defined

$$C(r_\rho, \sigma_1^p) \equiv \frac{\rho_{\rm loc}\,\sigma_1^p}{2\,(1+r_\rho)\,m_p^2}\,, \qquad \text{and} \qquad r_\sigma \equiv \frac{\sigma_2^p}{\sigma_1^p}\,. \tag{10}$$

$R_{A_2}(E_R)$ is similar, after making the following substitutions: $A_1 \to A_2$, $A_{1,1}^{\rm eff} \to A_{1,2}^{\rm eff}$ and $A_{2,1}^{\rm eff} \to A_{2,2}^{\rm eff}$. In the case of a DM signal generated from two components, it is clear that the particle masses will determine the slope of their individual rates, while r_ρ, r_σ and $\kappa_{1,2}$ will determine their relative normalisation. Therefore, a first conclusion is that using just information from a given direct detection signal, we can only distinguish if there are one or two components if the particles have different masses.

In the following numerical analysis, we will use different targets: fluorine, sodium, germanium and xenon. The strongest limits for the SI cross-section come from XENON1T [25], and are $10^{-45}\,{\rm cm}^2$ for a 10 GeV DM particle and $10^{-46}\,{\rm cm}^2$ for $m_{\rm DM} = 30$ GeV at 90% C.L. For SD couplings with protons, PICO-2L [26] (and PICO-60 [27] for heavier masses) set the strongest bounds, at the level of $10^{-40}\,{\rm cm}^2$ for a 10 GeV DM particle. The values of the energy threshold ($E_{\rm th}$), mass, time and exposures for the different nuclei based on future expected experimental sensitivities are given in table 1. Notice that there are many different proposed experiments, and very large uncertainties are present in the literature regarding these values. For Ge, although smaller thresholds are possible ($\lesssim$ keV), we take a conservative value similar to the other detector ones. Therefore our analysis can be understood as a proof of concept, with more sophisticated experimental simulations needed once there is a signal. We provide some examples of illustrative proposed experiments in the last column of the table. [2] We also provide in the third column the minimum DM mass that can be detected for each element assuming perfect energy resolution.

In Fig. 1 we show the differential spectrum of two component DM for a variety of DM mass splittings. One can see the different slopes of the two components and the presence of a kink in the total rate, which rapidly vanishes for smaller mass splittings. This is the smoking gun of multi-component DM. We have checked that sensible energy resolutions do not significantly affect the spectra, and in the following we assume perfect energy resolution and efficiency.

2.3 Test statistic for hypothesis testing

We construct the hypothesis test in a frequentist framework, defining the null hypothesis to be the one-component scenario which we denote $H_{\rm 1DM}$. Similarly we denote the two-component

[2] This is by no means an exhaustive list, and other elements and experiments are also very promising, for instance those using argon [28, 29], which however typically have higher energy thresholds ($\sim O(20)$ keV). Moreover, in addition to XENONnt [30], other very promising xenon experiments are DARWIN [31] and LZ [32]. For further details of the current status of DD experiments, the interested reader is referred to Refs. [33, 34].

Element	$E_{\rm th}$ (keV)	$m_{\rm DM}^{\rm min}$ (GeV)	M (t)	T (y)	MT ($t \cdot y$)	Experiments
F	3	2	0.5	2	1	PICO-500 [27]
Na	3	2.5	0.25	10	2.5	PICO-LON [35]
Ge	2	3.5	0.4	10	4	SuperCDMS [36]
Xe	1	3	2	1.5	3	XENONnT [30]

Table 1. Experimental values used in the numerical analysis for future direct detection experiments. Columns 2 to 6 show respectively the recoil energy threshold $E_{\rm th}$ (keV), the minimum DM mass that can be detected in GeV, the mass of the detector M in tonnes, the data collection time T in years and the total exposure MT ($t \cdot y$). The last column shows an illustrative experimental reference for the type of experiment considered. For xenon we consider both isotopes Xe^{129} and Xe^{131} with mass fractions x_j equal to 0.264 and 0.212, respectively.

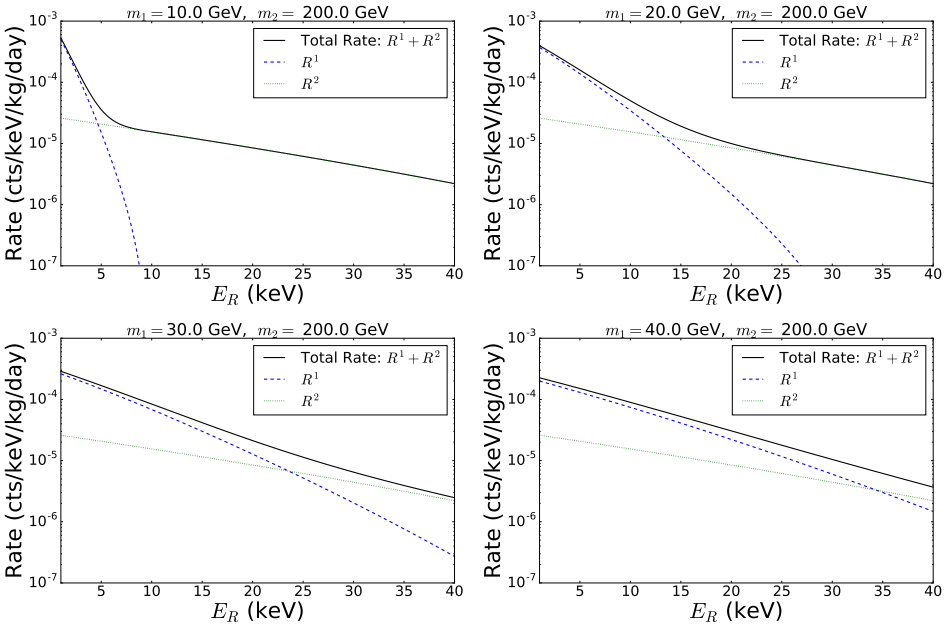

Figure 1. Total differential event rate for 2 DM particles (solid black), as well as their individual contributions (1 dashed blue, 2 dotted green) for a variety of DM mass splittings on the energy range [2, 30] keV. One should notice that the *kink* feature in the combined spectrum rapidly vanishes with smaller mass splittings.

alternative hypothesis $H_{\rm 2DM}$. Notice that the one DM hypothesis is a subset of the two DM hypothesis, as can be seen easily by taking $r_\rho = 0$ in Eq. (9). $H_{\rm 1DM}$ is said to be a *nested* hypothesis of $H_{\rm 2DM}$. We will see later that this has important ramifications.

Suppose that we have a detector that has observed a set of binned count measurements $\mathbf{x} = x_1, x_2 ..., x_N$ over N bins with uncertainties $\sigma_i = \sqrt{x_i}$. We parameterise the likelihood of observing this data given a hypotheses $H_{\rm 1DM}/H_{\rm 2DM}$ with a binned Gaussian distribution:

$$\mathcal{L}(\mathbf{x}\,|\,H_\alpha) = \prod_i^N \frac{1}{\sqrt{2\pi}\sigma_i} e^{-\frac{[x_i - \mu_i(\theta_\alpha)]^2}{2\sigma_i^2}} \qquad \alpha = [H_{\rm 1DM}, H_{\rm 2DM}], \tag{11}$$

where $\mu_i(\theta_\alpha)$ is the expected number of counts in bin i as a function of the model parameters $\theta_{H_{1\mathrm{DM}}}/\theta_{H_{2\mathrm{DM}}}$ under the hypothesis $H_{1\mathrm{DM}}/H_{2\mathrm{DM}}$. Maximising the likelihood in Eq. (11) with respect to the hypothesis parameters θ_α is equivalent to minimising -2 times the log-likelihood as follows:

$$\min_{\theta_\alpha}\left(-2\ln\mathcal{L}\right) = \min_{\theta_\alpha}\sum_{i}^{N}\frac{\left[x_i-\mu_i(\theta_\alpha)\right]^2}{\sigma_i^2} \equiv \min_{\theta_\alpha}\chi^2(\theta_\alpha)\,. \tag{12}$$

This is the familiar 'chi-square' statistic which, as showed by Pearson [37] in the limit of large x_i follows a χ^2 distribution with $N - n(\theta_\alpha)$ degrees of freedom, where $n(\theta_\alpha)$ is the number of parameters θ_α.

One should immediately notice that Eq. (12) only provides a 'goodness of fit' for the hypothesis α, and does not explicitly reject one in favour of the other. For this task, we require a test-statistic $\mathcal{T}$ that explicitly discriminates between $H_{1\mathrm{DM}}$ and $H_{2\mathrm{DM}}$. A commonly used test statistic is:

$$\mathcal{T} = \min_{\theta_{H_{1\mathrm{DM}}}}\chi^2(\theta_{H_{1\mathrm{DM}}}) - \min_{\theta_{H_{2\mathrm{DM}}}}\chi^2(\theta_{H_{2\mathrm{DM}}})\,. \tag{13}$$

Notice that the definition of $\mathcal{T}$ is such that the larger its value, the larger the preference for $H_{2\mathrm{DM}}$, and the smaller its value, the more $H_{1\mathrm{DM}}$ is preferred.

In order to quantify how much the data supports either hypothesis, we require the limiting probability distribution of the $\mathcal{T}$ statistic in the case either $H_{1\mathrm{DM}}$ and $H_{2\mathrm{DM}}$ is true. Under some general assumptions, the theorem from Wilk [38] states that in the case of nested hypotheses (i.e when $H_{1\mathrm{DM}}$ is true), $\mathcal{T}$ will follow a χ^2 distribution with $k \equiv n(\theta_{H_{2\mathrm{DM}}}) - n(\theta_{H_{1\mathrm{DM}}})$ degrees of freedom, where n is the number of parameters that parameterise a given hypothesis. We denote this by $\mathcal{T}^{1\mathrm{DM}}$.

However, in the case that $H_{2\mathrm{DM}}$ is true, we show in Appendix **??** that the $\mathcal{T}$ statistic, which we denote $\mathcal{T}^{2\mathrm{DM}}$, will follow a Gaussian distribution that is solely dependent on the true parameter values $\mu(\theta^{\mathrm{true}}_{H_{2\mathrm{DM}}})$ with mean given by $\mathcal{T}_0^{2\mathrm{DM}}$ and standard deviation $2\sqrt{\mathcal{T}_0^{2\mathrm{DM}}}$, where

$$\mathcal{T}_0^{2\mathrm{DM}} \equiv \mathcal{T}(x_i = \mu_i(\theta^{\mathrm{true}}_{H_{2\mathrm{DM}}})) = \min_{\theta_{H_{1\mathrm{DM}}}}\sum_{i}^{n}\left(\frac{\mu_i(\theta^{\mathrm{true}}_{H_{2\mathrm{DM}}}) - \mu_i(\theta_{H_{1\mathrm{DM}}})}{\sqrt{\mu_i(\theta^{\mathrm{true}}_{H_{2\mathrm{DM}}})}}\right)^2\,. \tag{14}$$

That is, $\mathcal{T}_0^{2\mathrm{DM}}$ has no statistical fluctuations from the data and is often called the *'Asimov likelihood'*. The Asimov likelihood can be qualitatively thought of as an approximation of the median value of a test statistic. See Ref. [39] for details. Note that large values of $\mathcal{T}_0^{2\mathrm{DM}}$ disfavour the null hypothesis $H_{1\mathrm{DM}}$.

In Fig. 2 we show the probability distribution of $\mathcal{T}$ for the two hypotheses in a Xe target: $H_{1\mathrm{DM}}$ in light red and $H_{2\mathrm{DM}}$ in light yellow. We fix $m_1 = 10$ GeV and $m_2 = 200$ GeV and use 8500 Monte Carlo samples. Since the only free parameters we are considering are the two DM masses, the difference in degrees of freedom of the two hypotheses is $k = 2 - 1 = 1$ degrees of freedom. Hence, from Wilk's theorem, we expect that under $H_{1\mathrm{DM}}$, $\mathcal{T}$ will follow a $\chi^2_{1\mathrm{d.o.f}}$ distribution. One can see that $\mathcal{T}^{2\mathrm{DM}}$ is approximately Gaussian distributed with median $\mathcal{T}_0^{2\mathrm{DM}}$ and standard deviation $2\sqrt{\mathcal{T}_0^{2\mathrm{DM}}}$, while $\mathcal{T}^{1\mathrm{DM}}$ is approximately estimated by a χ^2-distribution with one degree of freedom as expected.[3]

[3]One will also notice that the width of the Gaussian approximation in Fig. 2 slightly overestimates $\mathcal{T}^{2\mathrm{DM}}$. This of course could be primarily because we have assumed Monte Carlo realisations of the recoil spectrum are Gaussian distributed instead of Poisson. We have exploited the assumption that for large number of events the bin by bin distribution starts looking Gaussian. In practice, however, we are only interested in the median of the $H_{2\mathrm{DM}}$ distribution, since its variance does not enter in the calculation of the median sensitivity, as will be discussed in sec. 2.3.1.

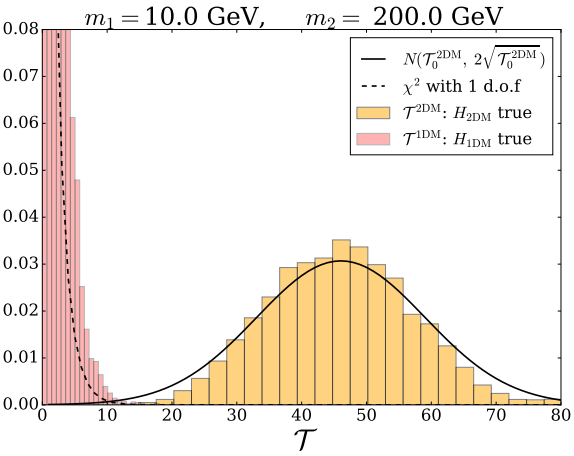

Figure 2. Normalised probability distribution of the test statistic $\mathcal{T}$ in a Xe target for true one-component $\mathcal{T}^{1DM}$ (light red) and two-component $\mathcal{T}^{2DM}$ (light yellow) DM hypothesis. We fixed $m_1 = 10$ GeV and $m_2 = 200$ GeV. We used 8500 samples. We see that the one-component DM follows a χ^2 distribution with one degree of freedom, while the two-component DM hypothesis is well-approximated by a Gaussian centered at $\mathcal{T}_0^{2DM}$, with standard deviation $2\sqrt{\mathcal{T}_0^{2DM}}$.

2.3.1 Median sensitivity

The aim of this analysis is to quantify how sensitive an "average experiment" operating at future benchmarks is to rejecting H_{1DM} in favour of H_{2DM}. The quantity that allows us to do this is called the *median sensitivity* and can be easily visualised as follows: Under H_{2DM} an experiment will generate a $\mathcal{T}^{2DM}$ statistic that is approximately Gaussian as shown in Fig. 2. In this vein, the median (mean) of this Gaussian $\mathcal{T}_0^{2DM}$ quantifies the experiments' 'average' capability.

Since we know that the distribution of $\mathcal{T}$ under H_{1DM} is a χ^2 with k degrees of freedom, we can then calculate the probability of having a $\mathcal{T}_0^{2DM}$ at least as extreme as the one we observed. This is called the *p-value* and is given by

$$p = \int_{\mathcal{T}_0^{2DM}}^{\infty} f(\mathcal{T}|H_{1DM})\, d\mathcal{T} = 1 - \mathrm{CDF}^{\chi^2}_{\mathrm{k\ d.o.f}}(\mathcal{T}_0^{2DM})\,, \tag{15}$$

where $\mathrm{CDF}^{\chi^2}_{\mathrm{k\ d.o.f}}$ is the cumulative density function for the $\chi^2_{k\ \mathrm{d.o.f}}$. As a result, a larger $\mathcal{T}_0^{2DM}$ which favours H_{2DM} will produce a smaller p-value, and vice-versa. We define α to be the probability of making an error of the 1st kind, i.e, rejecting H_{1DM} if its true. If $p < \alpha$, then the data supports H_{2DM} over H_{1DM}. In more conventional words, we have defined our critical region to be where there is a low probability to observe $\mathcal{T}$ if H_{1DM} is true but a high probabi1ity if the alternative hypothesis H_{2DM} is true. The p-value in Eq. (15) can be converted to a two-sided number of unit Gaussian standard deviations, which we will denote throughout the rest of this paper as Z, and call it the *median sensitivity* using [4]

$$Z(p) = \sqrt{2}\,\mathrm{erfc}^{-1}(\mathrm{p})\,, \tag{16}$$

[4] An alternate definition of the median sensitivity as seen in Ref. [40] is given by the CL at which an experiment will reject the wrong hypothesis with a probability of 50%, that is, with a rate for an error of the second kind of 0.5. We will use the definition in Eq. (16) for this study.

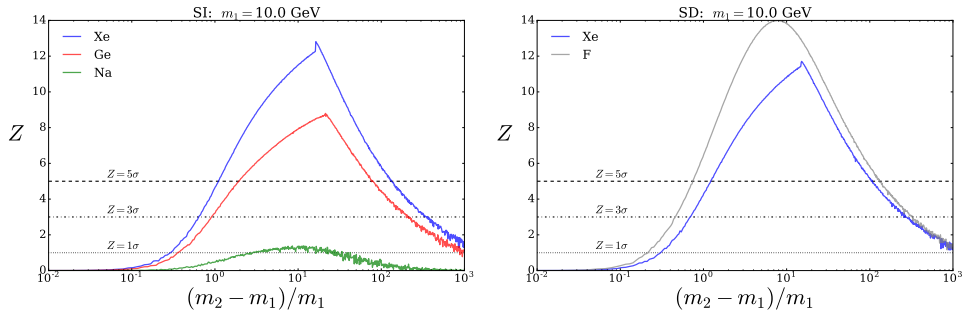

Figure 3. Significance Z with which the median experiment can reject the one-DM hypothesis in favour of the two-DM hypothesis as a function of the mass splitting $(m_2 - m_1)/m_1$, for fixed m_1 equal to 10 GeV. We show as dotted, dash-dotted and dashed (black) horizontal lines the 1, 3 and 5 σ C.L. The left panel shows the SI targets xenon (in blue), germanium (in red) and sodium (in green). The right panel shows the SD targets fluorine (in grey) and xenon (in blue).

where erfc(p) $\equiv 1 -$ erf(p) is the complimentary error function. If $Z \geq Z(\alpha) \equiv 5$ then the median experiment can reject $H_{1\text{DM}}$ in favour of $H_{2\text{DM}}$ at the 5-sigma confidence level (CL). In the special case that the difference in number of degrees of freedom is $k = 1$, the sensitivity is just given by [39]

$$Z|_{k=1} = \sqrt{\mathcal{T}_0^{2\text{DM}}} \,. \tag{17}$$

2.4 Fixed parameters except for the DM masses

We perform the analysis discussed in sec. 2.3 firstly for the case that all hypothesis parameters are fixed except for m_1 and m_2. As a result, the difference in number of degrees of freedom between $H_{1\text{DM}}$ and $H_{2\text{DM}}$ is $k = 1$. Thus, Eq. (17) is used in this case to calculate the median sensitivity.

For SI interactions we will consider future sodium, germanium and xenon experiments, with a true SI cross-section with protons of $\sigma^p_{1(\text{SI})} = 10^{-45}\,\text{cm}^2$. For SD interactions we will consider future fluorine and xenon experiments with true SD cross-section with protons of $\sigma^p_{1(\text{SD})} = 10^{-40}\,\text{cm}^2$. We adopt the experimental configurations shown in tab. 1. The choice of the nuclei for our assumed SI interaction experiments is such that there is a large range in masses, while for SD interactions there is an additional feature: fluorine (xenon) is most sensitive to DM couplings to protons (neutrons). We also assume a true (known) r_ρ, $r_\sigma = 1$, i.e., equal energy densities and cross-sections for the two DM particles, as well as equal couplings to protons and neutrons ($\kappa_{1,2} = 1$).

In order to illustrate how the mass splitting controls the hypothesis discrimination, we show in Fig. 3 the median significance Z as defined in Eq. (17) versus the normalised mass splitting $(m_2 - m_1)/m_1$, for a fixed lightest DM mass m_1 equal to 10 GeV. The left panel shows SI targets: xenon (in blue), germanium (in red) and sodium (in green). The right panel shows the SD targets fluorine (in grey) and xenon (in blue). We also show for reference the 1, 3, and 5 sigma contours as horizontal dotted, dash-dotted and dashed (black) lines. In the case of sodium, the significance is always very poor. This is due to two reasons. Firstly, the rate goes for spin-independent interactions as A^2. As a result, one obtains suppressed statistics in a Na based experiment as opposed to Xe and Ge when similar exposures are used. This dominates

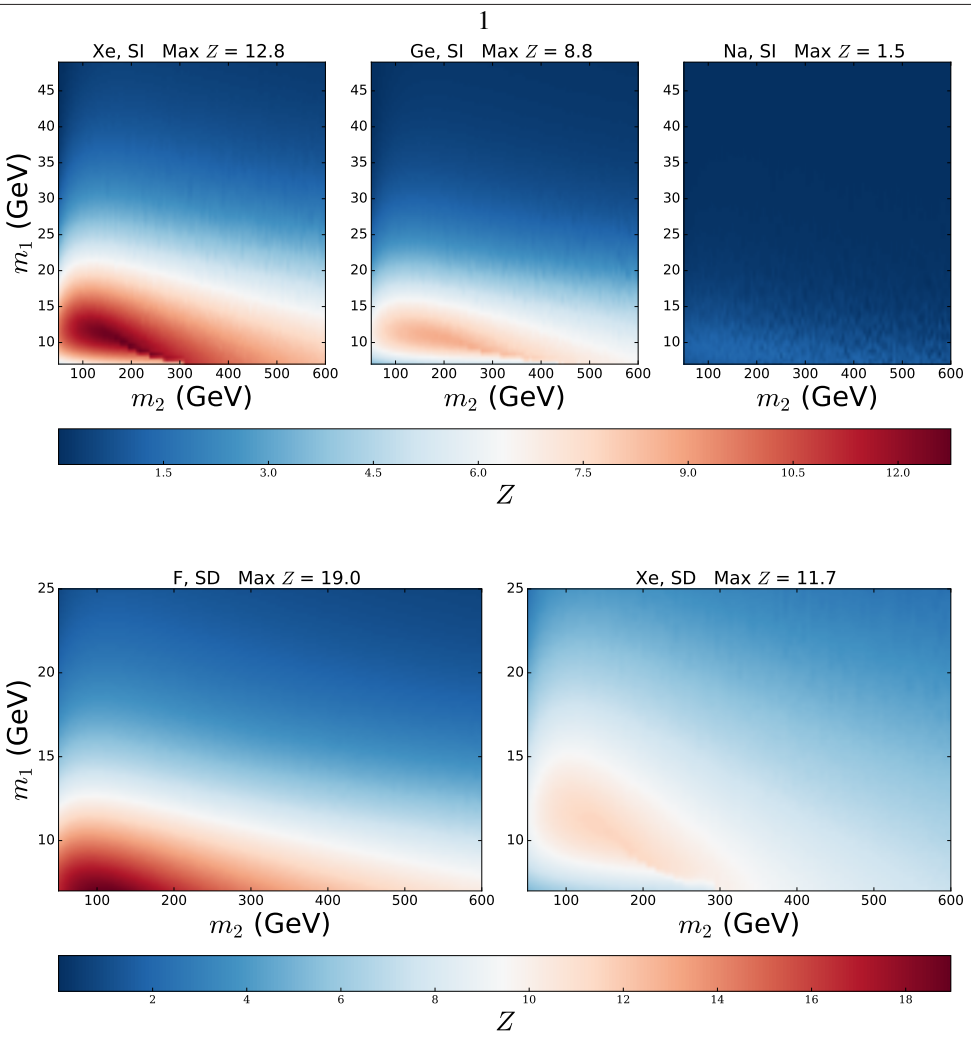

Figure 4. Significance Z with which the median experiment can reject the one-DM hypothesis in favour of the two-DM hypothesis in the $m_2 - m_1$ plane for different target nuclei. All other model parameters are fixed when generating the Asimov data: $r_\rho = r_\sigma = 1$, $\kappa_{1,2} = 1$ and $\sigma_{H_{1,2}} = 270$ km/s. We do not plot the symmetric region around the axis $m_1 = m_2$ for clarity. The top panel is for SI interactions for Xe, Ge and Na, while the bottom panel is for SD interactions for F and Xe.

the height of the curve in figure 6, left panel (c.f. figure 6 right panel for SD). Secondly, in general one is always more sensitive to recoils when roughly $m_{\rm DM} \sim m_{\rm Nucleus}$. Hence since one will only ever observe a significant 'kink' in the recoil spectrum for large enough mass splittings, a Na experiment will have trouble significantly rejecting the one-component hypotheses because it won't see the heavier particle. This effect is reflected by the relative shift of the peaks of the three curves (red, green and blue) in the left panel of figure 6. In all other cases, one should notice that the median significance is globally maximised at a mass splitting that is approximately equal to ~ 10 and drops to zero for very small $\lesssim 0.1$ or very

large $\gtrsim 10^3$ mass splittings. This illustrates that there exists only a finite window in masses, roughly $m_2 \sim O(1-100)\, m_1$, where there can be a significant ($\gtrsim 5\,\sigma$) discrimination.

In Fig. 4 we show the median sensitivity in the full mass plane $m_2 - m_1$. The top panel is for SI and the bottom panel for SD. One can see that the DM mass regions of large significance increase with the mass of the nucleus. Indeed, as discussed above, the significance for sodium is always negligible. Notice also that the regions shrink for very large masses of the heaviest DM, where its number density is so suppressed that it gives no signal in the detector. The exposure for such heavy masses is a critical factor to obtain a signal and achieve discrimination. For xenon, the largest sensitivity occurs when the lightest DM mass is around 10-20 GeV, and the heavy mass is in the range 50-400 GeV. For germanium, the largest significance occurs when the heaviest DM is lighter than roughly 300 GeV. For the SD case the main features are preserved for xenon, however the maximum significance that can be achieved is slightly lower. Fluorine however achieves maximum significance for m_2 in the range 50-200 GeV. Another feature of the SD fluorine result is that the median significance also drops above $m_1 \gtrsim 15$ GeV.

An important note to make is that the median (statistical) sensitivity scales as usual with the square root of the exposure

$$Z \propto \sqrt{MT}\ . \tag{18}$$

This is true for all detector types for both SI and SD interactions. This is important, since the results we show in this section can always be scaled accordingly for different experimental exposures to those given in tab. 1.

References

[1] J. Herrero-Garcia, A. Scaffidi, M. White, A.G. Williams, JCAP **1711**, 021 (2017), 1709.01945
[2] M.W. Goodman, E. Witten, Phys. Rev. **D31**, 3059 (1985)
[3] A. Adulpravitchai, B. Batell, J. Pradler, Phys. Lett. **B700**, 207 (2011), 1103.3053
[4] B. Batell, M. Pospelov, A. Ritz, Phys. Rev. **D79**, 115019 (2009), 0903.3396
[5] K.R. Dienes, J. Kumar, B. Thomas, Phys. Rev. **D86**, 055016 (2012), 1208.0336
[6] S. Profumo, K. Sigurdson, L. Ubaldi, JCAP **0912**, 016 (2009), 0907.4374
[7] S. Bhattacharya, P. Ghosh, T.N. Maity, T.S. Ray (2017), 1706.04699
[8] S. Bhattacharya, P. Poulose, P. Ghosh, JCAP **1704**, 043 (2017), 1607.08461
[9] D. Chialva, P.S.B. Dev, A. Mazumdar, Phys. Rev. **D87**, 063522 (2013), 1211.0250
[10] M. Blennow, S. Clementz, J. Herrero-Garcia, JCAP **1604**, 004 (2016), 1512.03317
[11] N. Bozorgnia, J. Herrero-Garcia, T. Schwetz, J. Zupan, JCAP **1307**, 049 (2013), 1305.3575
[12] D. Tucker-Smith, N. Weiner, Phys. Rev. **D72**, 063509 (2005), hep-ph/0402065
[13] G.F. Giudice, B. Gripaios, R. Mahbubani, Phys. Rev. **D85**, 075019 (2012), 1108.1800
[14] R.H. Helm, Phys. Rev. **104**, 1466 (1956)
[15] J. Lewin, P. Smith, Astroparticle Physics **6**, 87 (1996)
[16] P. Klos, J. Menéndez, D. Gazit, A. Schwenk, Phys. Rev. **D88**, 083516 (2013), [Erratum: Phys. Rev.D89,no.2,029901(2014)], 1304.7684
[17] G. Gelmini, P. Gondolo, Phys. Rev. **D64**, 023504 (2001), hep-ph/0012315
[18] C. Savage, K. Freese, P. Gondolo, Phys. Rev. **D74**, 043531 (2006), astro-ph/0607121
[19] K. Freese, M. Lisanti, C. Savage, Rev. Mod. Phys. **85**, 1561 (2013), 1209.3339

[20] J. Herrero-Garcia, T. Schwetz, J. Zupan, Phys. Rev. Lett. **109**, 141301 (2012), 1205.0134
[21] J. Herrero-Garcia, T. Schwetz, J. Zupan, JCAP **1203**, 005 (2012), 1112.1627
[22] S.K. Lee, M. Lisanti, A.H.G. Peter, B.R. Safdi, Phys. Rev. Lett. **112**, 011301 (2014), 1308.1953
[23] N. Bozorgnia, T. Schwetz, JCAP **1408**, 013 (2014), 1405.2340
[24] E. Del Nobile, G.B. Gelmini, S.J. Witte, JCAP **1508**, 041 (2015), 1505.07538
[25] E. Aprile et al. (XENON) (2017), 1705.06655
[26] C. Amole et al. (PICO), Phys. Rev. **D93**, 061101 (2016), 1601.03729
[27] C. Amole et al. (PICO), Phys. Rev. Lett. **118**, 251301 (2017), 1702.07666
[28] N. Fatemighomi (DEAP-3600), *DEAP-3600 dark matter experiment*, in *35th International Symposium on Physics in Collision (PIC 2015) Coventry, United Kingdom, September 15-19, 2015* (2016), 1609.07990, http://inspirehep.net/record/1488107/files/arXiv:1609.07990.pdf
[29] J. Calvo et al. (ArDM), JCAP **1703**, 003 (2017), 1612.06375
[30] E. Aprile et al. (XENON1T), JINST **9**, P11006 (2014), 1406.2374
[31] D.S. Akerib et al. (LZ) (2015), 1509.02910
[32] J. Aalbers et al. (DARWIN), JCAP **1611**, 017 (2016), 1606.07001
[33] T. Marrodán Undagoitia, L. Rauch, J. Phys. **G43**, 013001 (2016), 1509.08767
[34] J. Liu, X. Chen, X. Ji, Nature Phys. **13**, 212 (2017)
[35] K. Fushimi et al. (PICO-LON), J. Phys. Conf. Ser. **718**, 042022 (2016), 1512.04645
[36] R. Agnese et al. (SuperCDMS), Phys. Rev. **D95**, 082002 (2017), 1610.00006
[37] K.P. F.R.S., Philosophical Magazine **50**, 157 (1900), http://dx.doi.org/10.1080/14786440009463897
[38] S.S. Wilks, The Annals of Mathematical Statistics **9**, 60 (1938)
[39] G. Cowan, K. Cranmer, E. Gross, O. Vitells, The European Physical Journal C **71**, 1554 (2011)
[40] M. Blennow, P. Coloma, P. Huber, T. Schwetz, JHEP **03**, 028 (2014), 1311.1822